





# BRAIN COMMUNICATIONS

## Single-subject grey matter network trajectories over the disease course of autosomal dominant Alzheimer's disease

 Lisa Vermunt,<sup>1</sup>  Ellen Dicks,<sup>1</sup> Guoqiao Wang,<sup>2</sup> Aylin Dincer,<sup>3</sup> Shaney Flores,<sup>3</sup> Sarah J. Keefe,<sup>3</sup> Sarah B. Berman,<sup>4,5</sup> David M. Cash,<sup>6</sup> Jasmeer P. Chhatwal,<sup>7</sup> Carlos Cruchaga,<sup>8,9,10</sup> Nick C. Fox,<sup>11,12</sup> Bernardino Ghetti,<sup>13</sup> Neill R. Graff-Radford,<sup>14</sup> Jason Hassenstab,<sup>15,16,17</sup> Celeste M. Karch,<sup>8</sup> Christoph Laske,<sup>18,19</sup> Johannes Levin,<sup>20</sup> Colin L. Masters,<sup>21,22</sup> Eric McDade,<sup>15,16</sup> Hiroshi Mori,<sup>23</sup> John C. Morris,<sup>15,16</sup> James M. Noble,<sup>24</sup> Richard J. Perrin,<sup>15,25</sup> Peter R. Schofield,<sup>26,27</sup> Chengjie Xiong,<sup>2</sup> Philip Scheltens,<sup>1</sup> Pieter Jelle Visser,<sup>1,28</sup> Randall J. Bateman,<sup>8,15,16</sup> Tammie L. S. Benzinger,<sup>3,15</sup>  Betty M. Tijms<sup>1</sup> and  Brian A. Gordon<sup>3,15,17</sup>; on behalf of the Dominantly Inherited Alzheimer Network (DIAN)\*

The investigators of Dominantly Inherited Alzheimer Network (DIAN) are given in the Appendix I section.

Structural grey matter covariance networks provide an individual quantification of morphological patterns in the brain. The network integrity is disrupted in sporadic Alzheimer's disease, and network properties show associations with the level of amyloid pathology and cognitive decline. Therefore, these network properties might be disease progression markers. However, it remains unclear when and how grey matter network integrity changes with disease progression. We investigated these questions in autosomal dominant Alzheimer's disease mutation carriers, whose conserved age at dementia onset allows individual staging based upon their estimated years to symptom onset. From the Dominantly Inherited Alzheimer Network observational cohort, we selected T<sub>1</sub>-weighted MRI scans from 269 mutation carriers and 170 non-carriers (mean age 38 ± 15 years, mean estimated years to symptom onset -9 ± 11), of whom 237 had longitudinal scans with a mean follow-up of 3.0 years. Single-subject grey matter networks were extracted, and we calculated for each individual the network properties which describe the network topology, including the size, clustering, path length and small worldness. We determined at which time point mutation carriers and non-carriers diverged for global and regional grey matter network metrics, both cross-sectionally and for rate of change over time. Based on cross-sectional data, the earliest difference was observed in normalized path length, which was decreased for mutation carriers in the precuneus area at 13 years and on a global level 12 years before estimated symptom onset. Based on longitudinal data, we found the earliest difference between groups on a global level 6 years before symptom onset, with a greater rate of decline of network size for mutation carriers. We further compared grey matter network small worldness with established biomarkers for Alzheimer disease (i.e. amyloid accumulation, cortical thickness, brain metabolism and cognitive function). We found that greater amyloid accumulation at baseline was associated with faster decline of small worldness over time, and decline in grey matter network measures over time was accompanied by decline in brain metabolism, cortical thinning and cognitive decline. In summary, network measures decline in autosomal dominant Alzheimer's disease, which is alike sporadic Alzheimer's disease, and the properties show decline over time prior to estimated symptom onset. These data suggest that single-subject networks properties obtained from structural MRI scans form an additional non-invasive tool for understanding the substrate of cognitive decline and measuring progression from preclinical to severe clinical stages of Alzheimer's disease.

Received January 16, 2020. Revised May 25, 2020. Accepted June 18, 2020. Advance Access publication July 15, 2020

© The Author(s) (2020). Published by Oxford University Press on behalf of the Guarantors of Brain.

This is an Open Access article distributed under the terms of the Creative Commons Attribution Non-Commercial License (<http://creativecommons.org/licenses/by-nc/4.0/>), which permits non-commercial re-use, distribution, and reproduction in any medium, provided the original work is properly cited. For commercial re-use, please contact [journals.permissions@oup.com](mailto:journals.permissions@oup.com)

- 1 Department of Neurology, Amsterdam Neuroscience, Alzheimer Center Amsterdam, Amsterdam, UMC, VU University, Netherlands
- 2 Division of Biostatistics, Washington University in St. Louis, MO, USA
- 3 Mallinckrodt Institute of Radiology, Washington University in St. Louis, MO, USA
- 4 Department of Neurology, Alzheimer's Disease Research Center, Pittsburgh, PA
- 5 Pittsburgh Institute for Neurodegenerative Diseases, University of Pittsburgh, Pittsburgh, PA
- 6 UCL Queen Square Institute of Neurology, London, UK
- 7 Department of Neurology, Massachusetts General Hospital, Boston, MA, USA
- 8 Department of Psychiatry, Washington University in St. Louis, MO, USA
- 9 Hope Center for Neurological Disorders, . Washington University in St. Louis, MO, USA
- 10 NeuroGenomics and Informatics, Washington University in St. Louis, St. Louis, MO, USA
- 11 Dementia Research Centre, Department of Neurodegenerative Disease, UK
- 12 Dementia Research Institute at UCL, UCL Institute of Neurology, London, UK
- 13 Department of Pathology and Laboratory Medicine, Indiana University, IN, USA
- 14 Mayo Clinic Florida, FL, USA
- 15 Knight Alzheimer's Disease Research Center, Washington University in St. Louis, MO, USA
- 16 Department of Neurology, Washington University in St. Louis, MO, USA
- 17 Department of Psychological & Brain Sciences, Washington University in St. Louis, MO, USA
- 18 German Center for Neurodegenerative Diseases (DZNE), Tübingen, Germany
- 19 Section for Dementia Research, Hertie Institute for Clinical Brain Research and Department of Psychiatry and Psychotherapy, University of Tübingen, Germany
- 20 Ludwig-Maximilians-Universität München, Germany
- 21 Florey Institute, Melbourne, Australia
- 22 The University of Melbourne, Melbourne, Australia
- 23 Department of Clinical Neuroscience, Osaka City University Medical School, Japan
- 24 Department of Neurology, Taub Institute for Research on Alzheimer's Disease and the Aging Brain, GH Sergievsky Center, Columbia University Medical Center, NY, USA
- 25 Department of Pathology and Immunology, Washington University School of Medicine, St. Louis MO, USA
- 26 Neuroscience Research Australia, Sydney, Australia
- 27 School of Medical Sciences, UNSW Sydney, Sydney, Australia
- 28 Department of Psychiatry and Neuropsychology, Maastricht University, School for Mental Health and Neuroscience, Alzheimer Center Limburg, Netherlands

Correspondence to: Lisa Vermunt, MD, PhD

Department of Neurology

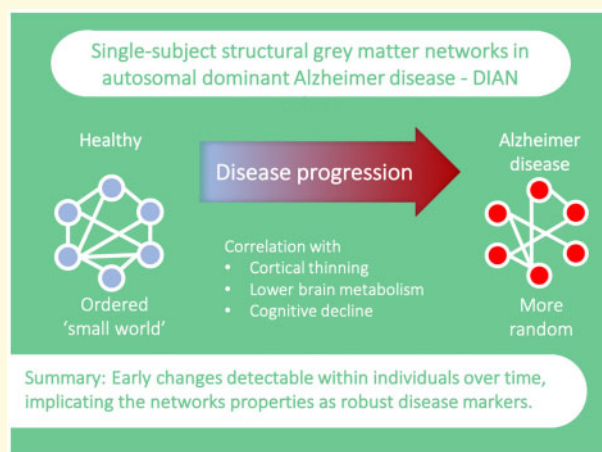
Amsterdam Neuroscience, Alzheimer Center Amsterdam, Amsterdam UMC, Vrije Universiteit, Netherlands

E-mail: l.vermunt@amsterdamumc.nl

**Keywords:** autosomal dominant; Alzheimer's disease; disease progression; network; subject-level networks

**Abbreviations:**  $A\beta$  = amyloid  $\beta$ ; ADAD = autosomal dominant Alzheimer's disease; *APP* = amyloid precursor protein gene; CDR = Clinical Dementia Rating scale; DIAN = Dominantly Inherited Alzheimer Network; EYO = estimated years to symptom onset; FDG = 18F-Fluorodeoxyglucose; *PSEN* = *Presenilin* gene; ROI = region of interest; SPM = Statistical Parametric Mapping software; SD = standard deviation; SUVR = standardized uptake value ratio.

## Graphical Abstract



## Introduction

In order to advance clinical trials to slow or halt Alzheimer's disease, the most frequent cause of dementia (Scheltens *et al.*, 2016), it is important both to understand the evolution of pathophysiological changes occurring and to develop disease progression markers (Aisen *et al.*, 2017). Current biomarkers reliably detect Alzheimer's disease pathology (Jack *et al.*, 2018), however, predicting and monitoring disease progression remain difficult. Brain network properties are linked to cognitive function (Bassett and Bullmore, 2009; Chhatwal *et al.*, 2018; Franzmeier *et al.*, 2018), therefore studying network integrity may offer new insights into disease progression in Alzheimer's disease.

One way to measure of brain networks is by determining the similarity of grey matter morphological measures between brain regions across individuals, i.e. grey matter covariance networks (He *et al.*, 2008; Li *et al.*, 2012; Tijms *et al.*, 2012) (Fig. 1). This approach is based on the notion that brain regions involved in distinct cognitive functions tend to develop in a similar way, possibly due to shared neurotrophic factors (Zielinski *et al.*, 2010; Alexander-Bloch *et al.*, 2013a, b). Common developmental trajectories and functional co-activation result in similar grey matter tissue properties, as measured on structural MRI (Draganski *et al.*, 2004; Mechelli *et al.*, 2005; Seeley *et al.*, 2009). These covariance patterns are related to normal cognition (Seidlitz *et al.*, 2018; Doucet *et al.*, 2019) and reveal in healthy individuals an optimal, 'small-world', organization by graph theory description (He *et al.*, 2007; Humphries and Gurney, 2008). In sporadic Alzheimer's disease dementia, grey matter networks are disrupted, the properties show a less optimal, random organization of the network (Yao *et al.*, 2010; Tijms *et al.*, 2013a; Kim *et al.*, 2016). In pre-dementia stages, such loss of network integrity predicts clinical progression and cognitive decline (Dicks *et al.*, 2018; Tijms *et al.*, 2018). The presence of amyloid  $\beta$  ( $A\beta$ ) pathology in cognitively normal individuals has also been associated with grey matter network alterations (Tijms *et al.*, 2016; Ten Kate *et al.*, 2018; Voevodskaya *et al.*, 2018). Together, these observations suggest that these network properties change over the course of Alzheimer's disease, from early stages, and that individual grey matter network extractions could possibly be used to monitor disease progression. However, as previous findings were based on one-time network extractions, it remains unclear whether, and when, these networks change *within* individuals as they progress in their disease.

A complication when studying sporadic Alzheimer's disease is the difficulty of placing pre-symptomatic individuals on their disease timeline (Villemagne *et al.*, 2013; Donohue *et al.*, 2014; Young *et al.*, 2014; Roe *et al.*, 2018; Vermunt *et al.*, 2019). This issue is less problematic for carriers of a genetic mutation that causes autosomal dominant Alzheimer's disease (ADAD), because the

age at onset of dementia can be estimated, from the age at onset in family members or carriers of the same specific mutation type. The estimated years to symptom onset (EYO) can serve as a proxy for disease duration (Bateman *et al.*, 2012; Ryman *et al.*, 2014). Using this paradigm, previous work demonstrated that  $A\beta$  aggregation starts more than two decades before dementia onset (Gordon *et al.*, 2018; McDade *et al.*, 2018; Oxtoby *et al.*, 2018). Closer to symptom onset, individuals show accelerated hypometabolism and cortical thinning, which is followed by cognitive decline (Benzinger *et al.*, 2013; Kinnunen *et al.*, 2018; Wang *et al.*, 2019). When during these processes, grey matter networks start to decline remains unknown.

Here, we investigated for the first time single-subject grey matter networks over the course of ADAD. We assessed when, and how, the network properties change as a function of EYO, both cross-sectionally and longitudinally, on a global and regional level. To understand the relationship between grey matter network property changes and disease progression, we also investigated how the network small-world coefficient alters with established Alzheimer's disease markers of  $A\beta$  accumulation, brain metabolism, cortical thickness and cognitive function.

## Materials and methods

### DIAN study design and participants

In the worldwide Dominantly Inherent Alzheimer Network (DIAN) longitudinal cohort study, families with individuals carrying a *PSEN1*, *PSEN2* or *APP* mutation undergo genetic testing and repeated clinical, cognitive, fluid and brain imaging assessments. The non-carrier family members act as an inherent control group. Participants generally have study visits every 3 years at earlier disease stages and these assessments become yearly when either symptoms are present, or they are within 3 years of their EYO. DIAN protocols had supervisory approval from the ethical review board of Washington University in St. Louis, and all participants gave informed consent. For this study, we selected data from all participants who had undergone at least one MRI scan that passed quality control in the 12th data freeze. Families with the Dutch or Flemish *APP* mutation were excluded because these mutations result in a different phenotype, with predominantly cerebral amyloid angiopathy.

### Estimated years to symptom onset

We calculated the EYO for mutation carriers and non-carriers identically: The EYO was defined as the mutation-specific mean age at onset subtracted by the individuals' visit age (Ryman *et al.*, 2014). In case of an unknown mutation-specific age at onset, the parental age at disease onset, reported by the participant, was used

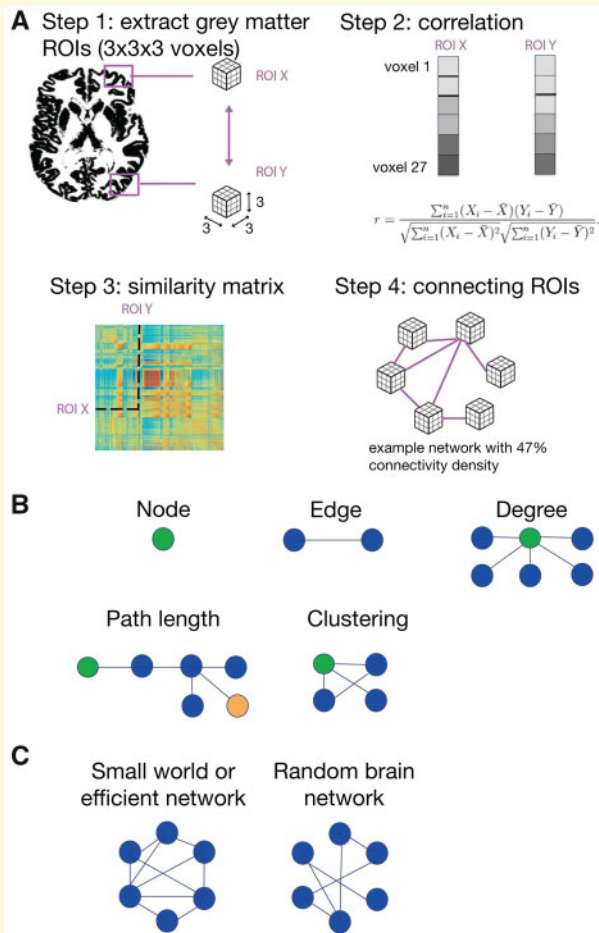


**Figure 1** Details on grey matter network metrics. (With permission from Verfaillie et al. 2018, Human Brain Mapping.) (A) Grey matter network extraction from the individual brain segmentation (described in text). (B) The sum of the number of nodes, i.e. the number of cubes, is the size of the network. The *degree* is the average number of connections per node. The *connectivity density* is the percentage of the number of connections in the network compared to the maximum number of connections possible. The *clustering coefficient* of a node describes the proportion of connections between neighbours for every node. For example, in case a node connects to 3 other nodes, there are 3 possible connections between those 3 adjacent nodes. If only 1 connection is present between 2 of the 3 other nodes, the clustering of the primary node is 1 out of 3, 0.33. Global clustering is determined by taking averaging clustering values across all nodes. *Path length* is the mean of the shortest paths for a node to reach every other node in the network. The global path length is the average path length across all nodes. (C) *Normalized clustering* and *normalized path length* describe how on a global level a network organization differs from a randomly organized network. The networks are randomized by rewiring the connections randomly in each network, while keeping intact the total number of nodes and degrees (Maslov and Sneppen, 2002). The network's observed clustering and path length are divided by the clustering and path length values, respectively, of averaged random networks to obtain the normalized values. Lastly, the *small-world coefficient* is the normalized clustering divided by the normalized path length. The network has the 'small-world property' if this ratio is higher than 1, indicating a path length close to the random networks, yet a greater

then random clustering. This is optimal, because of fast exchange of information between remote clusters, and specialized information processing within clusters.

instead. For example, if the mean age at symptom onset for a specific mutation is 50 years, then a 35-year-old individual would have an EYO of  $-15$ . For the carriers of the ADAD mutation, this indicates that the individual is expected to show clinical symptoms of Alzheimer's disease 15 years later.

## Clinical evaluation and cognition

Disease severity was measured using the Clinical Dementia Rating scale (CDR) (Morris, 1993), administered to the participant and study partner by blinded raters. Participants were classified as being unimpaired (global CDR score = 0) or symptomatic (global CDR 0.5, 1, 2 and 3). In addition, cognitive function was summarized using a cognitive composite developed in the DIAN project (Bateman et al., 2017), consisting of the average of equally weighted Z-scores of the Logical Memory delayed recall total score from the Wechsler Memory Scale-Revised, DIAN Word List Test delayed free recall score, Digit Symbol Coding total score from the Wechsler Adult Intelligence Scale-Revised Digit Symbol Substitution Test, and the total score from the Mini-Mental State Examination.

## MRI acquisition and pre-processing

MRI T<sub>1</sub>-weighted scans (1.1×1.1×1.2 mm<sup>3</sup> voxels, repetition time = 2300 ms, echo time = 2.95 ms, flip angle 9°) were acquired according to Alzheimer's Disease Neuroimaging Initiative (ADNI) protocols (Jack et al., 2010). We segmented T<sub>1</sub> images into grey and white matter and CSF, using the Statistical Parametric Mapping software version 12 (SPM12; Wellcome Trust Centre for Neuroimaging, UCL Institute of Neurology, London, UK). All segmentations were checked visually, after which 51 scans were removed due to failed segmentations or severe motion artefacts. Native space grey matter segmentations were resampled into 2 × 2 × 2 mm<sup>3</sup> voxels. This voxel-wise data were used as input for connectivity analyses.

## Single-subject grey matter networks and metrics

Grey matter networks were computed according to a previously published, automated pipeline (Tijms et al., 2012) that includes two steps figured in Fig. 1A: (i) grey matter network extraction (<https://github.com/bettytijms/Single-Subject-Grey-Matter-Networks>, accessed December 2019; implemented in Matlab2016b (MathWorks, Natick, MA)) and (ii) graph theory-based metric calculation (Rubinov and Sporns, 2010; Tijms et al., 2012). To extract single-

subject grey matter networks, we parcellated each individual's native space grey matter segmentation into  $6 \times 6 \times 6$  mm<sup>3</sup> cubes, containing 27 voxels. These non-overlapping cubes serve as the 'nodes' in the network. Connections between each pair of cubes across an individual's scan were established by calculating the Pearson's correlation coefficient between the corresponding voxels. This approach takes into account both the grey matter probability (i.e. from the tissue segmentation) as well as the spatial information present in 27 voxels within each cube. All correlations were stored in a matrix, and the presence or absence of connections between nodes was dichotomized according to an individualized threshold that ensured a maximum of 5% spurious connections for each individual (Tijms *et al.*, 2012).

For each individual's binarized grey matter network, we calculated graph theory metrics describing the global network properties: size, degree, connectivity density, clustering coefficient, path length, normalized clustering, normalized path length and small-world coefficient (see Fig. 1B and C for explanation of these metrics). We also calculated regional network properties. In order to aid comparability with other studies previously performed in DIAN, regional network metrics were calculated within each region of the Desikan-Killiany atlas (Desikan *et al.*, 2006). The regional masks were obtained by first parcellating each individual's T<sub>1</sub> image into 34 anatomical regions of interest (ROIs) from the Desikan atlas using Freesurfer 5.3 (Fischl, 2012) (<http://surfer.nmr.mgh.harvard.edu>, accessed December 2019). The Freesurfer output was then aligned to the native space T<sub>1</sub> using FSL (<https://fsl.fmrib.ox.ac.uk/fsl>, accessed December 2019), and this transform was used to register the parcellation into native space. The network values of the degree, clustering coefficient and path length were subsequently averaged within a region. Graph theory metrics were calculated using scripts from the brain connectivity toolbox (<https://sites.google.com/site/bctnet/>, accessed December 2019), modified for large-sized networks.

## Other DIAN imaging data

We examined regional data for A $\beta$  using PET imaging with 11 C-Pittsburgh Compound B (A $\beta$  PET), glucose metabolism with 18F-Fluorodeoxyglucose PET (FDG-PET), and cortical thickness and volumes from structural MRI. Details on data processing have previously been described (Gordon *et al.*, 2018). The Freesurfer ROIs were used to process the amyloid and FDG-PET data. PET data are processed using a cerebellar grey reference region and partial volume corrected using a geometric transfer matrix approach (Su *et al.*, 2013; Su *et al.*, 2015). In this study, we utilized the MRI precuneus cortical thickness, the precuneus A $\beta$  PET and to match a previously defined meta-ROI, the average of the left and right isthmus cingulate and inferior parietal region in FDG-PET for cross-

modal comparison with grey matter network properties (Landau *et al.*, 2011).

## Statistical analyses

As part of sample characterization, we compared four groups (non-carriers; asymptomatic mutation carriers with an EYO before -15 years; asymptomatic mutation carriers with EYO between -15 and 0 years; and symptomatic mutation carriers) on cross-sectional grey matter network small-world values, and the other network measures with the Kruskal-Wallis test, and *post hoc* Wilcoxon test with Holm *P*-value adjustment. We extracted individual slopes with linear mixed models in R for those individuals with repeated measures. Using the same statistical tests, we compared those extracted slopes between the groups. In addition, we compared individuals with different mutation types (PSEN1/PSEN2/APP) on the baseline network property values.

For the main analyses, we compared mutation carriers and non-carriers to determine (i) the EYO at which grey matter network metrics showed cross-sectional differences between groups and (ii) the EYO at which the groups had a different rate of change over time by fitting linear mixed effects models. Specifically, we used Bayesian inference methods (Gordon *et al.*, 2018; Mishra *et al.*, 2018) to determine the EYO point that 99% credible intervals of the difference distribution did not overlap 0. In these methods, the model parameters were estimated as previously described, applying a Hamiltonian Markov chain Monte Carlo sampling of the posterior distribution, with 10 000 iterations in eight chains, 5000 warm-up, thinning retaining 1 out of every 10 iterations and cauchy prior in the STAN package for R. We checked the model convergence statistic Gelman-Rubin diagnostic, the  $\hat{R}$ -statistic (rhat), which compares the between and within-chain estimates for each of the model parameters. These should be at least close to 1.0 and were for all models close to 1.00. (Gelman *et al.*, 2015; Carpenter *et al.*, 2017). From the posterior distribution, we calculated the range 99% credible intervals around the estimates, i.e. 0.005–0.995 range. We also calculated the difference curve between the mutation carriers and non-carriers by EYO with 99% credible intervals. We refer to the 'divergence point' as the point where the 99% credible interval of this difference curve between carriers and non-carriers did not contain 0 (i.e. no difference). The credible interval is the Bayesian equivalent of the frequentist confidence interval. The main difference is that the Bayesian directly estimates the credible interval from an actual computed population (i.e. posterior) distributions, rather than hypothesized as in the frequentists approach. Therefore, an advantage of the Bayesian approach is that the credible interval can be interpreted in a probabilistic way. To allow for non-linear effects, without assuming a particular shape, we applied a restricted cubic spline with knots at the 0.10, 0.50 and 0.90 of the EYO

distribution, also described previously (Gordon *et al.*, 2018) that included a linear term (EYOlinear) and a cubic term (EYOcubic). Cross-sectional models contained fixed terms for EYO, mutation status, their interaction and a random effect for family cluster. Longitudinal models were used to study the rate of change of network properties, and individuals with one data point were also included. Those models included fixed terms for baseline EYO (two terms: EYOlinear and EYOcubic), time after baseline, mutation status and, all two- and three-way interactions (see formulas in [Supplementary material](#), p. 6). Additionally, all models included random intercept terms for subject and family cluster and a random slope for subject. The covariates whole-brain grey matter volume and sex were included as fixed terms. Equivalent to previous work, when size, degree or connectivity density were found to be associated with mutation status in any of the models, were included as additional covariates for sensitivity analysis as these variables also influence more complex network metrics (Tijms *et al.*, 2013a). Regional models were adjusted for sex, regional degree and regional grey matter volume.

We examined relationships between grey matter network small-world coefficient and established Alzheimer's disease markers within mutation carriers. Previous research suggested grey matter networks may be disrupted in response to  $A\beta$  accumulation, precipitating cognitive decline (Ten Kate *et al.*, 2018). For this reason, our models included either precuneus PET  $A\beta$  as a predictor and grey matter network metrics as outcomes or grey matter network metrics as a predictor and cortical thickness (precuneus), brain metabolism (meta-ROI), or cognition (DIAN cognitive composite) as the respective outcomes. These predictors and outcomes were Z-scored to the whole group. We fitted three sets of linear mixed effects models that were all adjusted for baseline grey matter volume, age, and sex, and with random intercept for family cluster, in lme4 package in R (Bates *et al.*, 2014) (see detailed formulas in [Supplementary material](#), p. 6). If models failed to converge, the term for family cluster was removed. Models were divided into three sections. The first was baseline comparisons. The second set was longitudinal comparisons in participants with at least two data points to avoid convergence issues and included additional random effects for subject intercept and slope of the predictor. The final set of models was used to evaluate whether baseline data could predict change over time in the outcome. These models had fixed effects for baseline predictor, time from baseline, and its interaction, and a random subject intercept and slope of time from baseline. We focused on the grey matter network small-world coefficient, as this metric is indirectly derived from all other network metrics, and can thus be considered a summary statistic (Fig. 1). We also show exploratory graphs for the other network measures for completeness and repeated as a sensitivity analysis the cross-modal models for the mutation carriers only.

## Data availability

The data from the DIAN study can be requested online at <https://dian.wustl.edu/>, accessed December 2019.

## Results

In total, 439 participants from the DIAN study, with a mean  $\pm$  SD age of  $38 \pm 11$  years and a mean  $\pm$  SD EYO of  $-9 \pm 11$ , had MRI scans of sufficient quality to be included in the present analyses. The group consisted of 269 (61%) ADAD mutation carriers and 170 (39%) non-carrier family members (Table 1). Of this sample, 237 (54%) participants had longitudinal MRI scans, with a mean of 2.5 scans per participant and a maximum of 6 acquired over a mean  $\pm$  SD  $3.0 \pm 1.5$  years of follow-up (clinical and PET data in [Supplementary Table 1](#)). There were group differences between asymptomatic mutation carriers with  $EYO < -15$  years, asymptomatic mutation carriers  $-15 < EYO < 0$  years, symptomatic mutation carriers and non-carriers on cross-sectional network values and extracted slopes ([Supplementary Figs 3 and 4](#)). For most network measures, we found that the mutation carriers who are far away from expected onset ( $EYO > 15$  years) and the non-carriers had slightly higher network property value than mutation carriers who were closer to expected symptom onset, and it further decreased in the symptomatic stage. Rate of decline showed a similar pattern between these groups. Figure 2 illustrates these comparisons for the small-world coefficient. Comparing *PSEN1/PSEN2/APP* mutation carriers at baseline on all network metrics, the network size and average degree were slightly lower in *PSEN1* carriers, while the other metrics were similar ([Supplementary Fig. 5](#)).

## Cross-sectional divergences between mutation carriers and non-carriers

The mutation carriers diverged from non-carriers on all grey matter network metrics, except for network size and raw path length (Fig. 3, [Supplementary Table 2](#)). Lower network metric values for mutation carriers relative to non-carriers were observed earliest in normalized path length at  $EYO -12$ , followed by lower normalized clustering at  $EYO -8.7$ , small-world coefficient at  $EYO -8.4$ , clustering coefficient at  $EYO -7.5$ , connectivity density at  $EYO -5.6$  and degree at  $EYO 0$ . When additionally adjusting for degree or connectivity density, the estimates for network metrics yielded similar results ([Supplementary Table 2](#)). Using the same methods, but now implemented on a regional level, the earliest divergence between mutation carriers relative to non-carriers was found for path length in the precuneus at  $EYO -13.1$ , for clustering in the superior temporal gyrus at  $EYO -10$  and for network degree in the banks of the superior temporal gyrus at  $EYO -7$  (Fig. 4, [Supplementary Table 3](#)).

## Divergences of rates of change between mutation carriers compared to non-carriers

When comparing rates of change over time, mutation carriers diverged from non-carriers by EYO for all grey matter network metrics, except connectivity density. Steeper decline for mutation carriers relative to non-carriers was detected earliest for network size, at baseline EYO  $-6.0$ , followed by small-world coefficient at EYO  $-4.7$ , normalized clustering at EYO  $-4.6$ , degree at EYO  $-4.4$ , normalized path length at EYO  $-2.8$ , clustering coefficient at EYO  $-2.6$  and path length at  $+1.0$  (Fig. 2, Supplementary Table 2 and Figs 1 and 2). When additionally adjusting for degree, the estimates for network metrics yielded similar results, except for clustering coefficient, which lost significance. On a regional level, the earliest steep decline rate for mutation carriers compared to non-carriers was detected for degree in the lateral occipital gyrus at EYO  $-7.4$ , for clustering in the parahippocampal gyrus at EYO  $-6.2$  and for path length in the precentral gyrus at EYO  $-4.2$ . (Fig. 4, Supplementary Table 3).

## Association of grey matter networks with other neuroimaging and cognition

Established markers of Alzheimer's disease showed significant relationships with the small-world coefficient used as a global network summary statistic. We examined cross-modal relationships between baseline markers; over repeated measures; and whether baseline values could predict further decline in the other marker. We found that higher  $A\beta$  deposition load on PET was cross-sectionally related to a lower small-world coefficient ( $\beta \pm SE = -0.22 \pm 0.05$ ,  $P = 3 \times 10^{-6}$ , Fig. 5). In a longitudinal design, faster amyloid accumulation over time related to concurrent small-world coefficient decline ( $\beta \pm SE = -0.33 \pm 0.06$ ,  $P = 1 \times 10^{-7}$ ). Thirdly, a higher amyloid load at baseline predicted steeper decline of the small-

world coefficient over time ( $\beta \pm SE = -0.07 \pm 0.01$ ,  $P = 4 \times 10^{-8}$ ).

Grey matter network small-world coefficient and the markers of Alzheimer's disease progression showed significant relationships, both cross-sectionally and longitudinally (Fig. 6). Specifically, a lower small-world coefficient was cross-sectionally related to lower FDG-PET metabolism in the meta-ROI ( $\beta \pm SE = 0.44 \pm 0.08$ ,  $P = 2 \times 10^{-7}$ ), as well as lower precuneus cortical thickness ( $\beta \pm SE = 0.50 \pm 0.06$ ,  $P = 2 \times 10^{-15}$ ). For cognition, a lower small-world coefficient was cross-sectionally related to lower scores on the DIAN cognitive composite ( $\beta \pm SE = 0.28 \pm 0.08$ ,  $P = 3 \times 10^{-4}$ ). In a longitudinal design, decline of the small-world coefficient over time related to concurrent decreases of FDG-PET metabolism ( $\beta \pm SE = 0.54 \pm 0.06$ ,  $P = 5 \times 10^{-14}$ ) and faster precuneus cortical thinning ( $\beta \pm SE = 0.55 \pm 0.06$ ,  $P = 1 \times 10^{-17}$ ). A declining small-world coefficient over time was related to concurrent decline on the cognitive composite ( $\beta \pm SE = 0.47 \pm 0.06$ ,  $P = 2 \times 10^{-11}$ ). Thirdly, a lower small-world coefficient at baseline predicted faster neurodegeneration as measured by FDG-PET metabolism ( $\beta \pm SE = 0.12 \pm 0.02$ ,  $P = 2 \times 10^{-8}$ ) and precuneus cortical thinning ( $\beta \pm SE = 0.10 \pm 0.01$ ,  $P = 4 \times 10^{-12}$ ), and steeper cognitive decline over time (composite  $\beta \pm SE = 0.08 \pm 0.02$ ,  $P = 2 \times 10^{-7}$ ). Associations for the other network properties can be found in Supplementary Figs 6–9 in explorative graphs.

We repeated the cross-modal analyses, this time solely including the mutation carriers who were asymptomatic at baseline (see Supplementary Table 4). In brief, most relationships, albeit attenuated, were also present in the asymptomatic mutation carriers only. The cross-sectional relationships with the small-world coefficient remained significant for FDG-PET metabolism and precuneus cortical thickness. All longitudinal relationships indicating concurrent changes between markers were significant. Of the third set of models, aimed at predicting the change over time, two models did not converge (with amyloid PET and with cognition). The baseline small-world property still predicted the decline of FDG-PET metabolism.

**Table 1** Group characteristics

	Non-carriers (N = 170)	Asymptomatic mutation carriers (N = 174)	Symptomatic mutation carriers (N = 95)
Baseline age, years	38 (11)	34 (9)	46 (10)
Female, N (%)	101 (59%)	100 (57%)	50 (53%)
Estimated years to onset	-11 (12)	-14 (8)	1 (7)
MMSE	29.1 (1.2)	29.1 (1.2)	22.9 (6.6)
Total MRI scans, 1/2/3/4-6, N	84/61/18/7	84/59/28/3	34/30/17/14
Longitudinal scans, mean (SD)	2.4 (0.8)	2.4 (0.7)	2.9 (1.1)
Follow-up time MRI visits, years	3.3 (1.5)	3.2 (1.5)	2.2 (1.3)
Mutation type, PSEN1/PSEN2/APP, N	n/a	133/16/25	75/2/18

Mean (SD), unless otherwise specified. EYO is the expected age at onset of the mutation that runs in the family. MMSE = Mini-Mental State Examination.

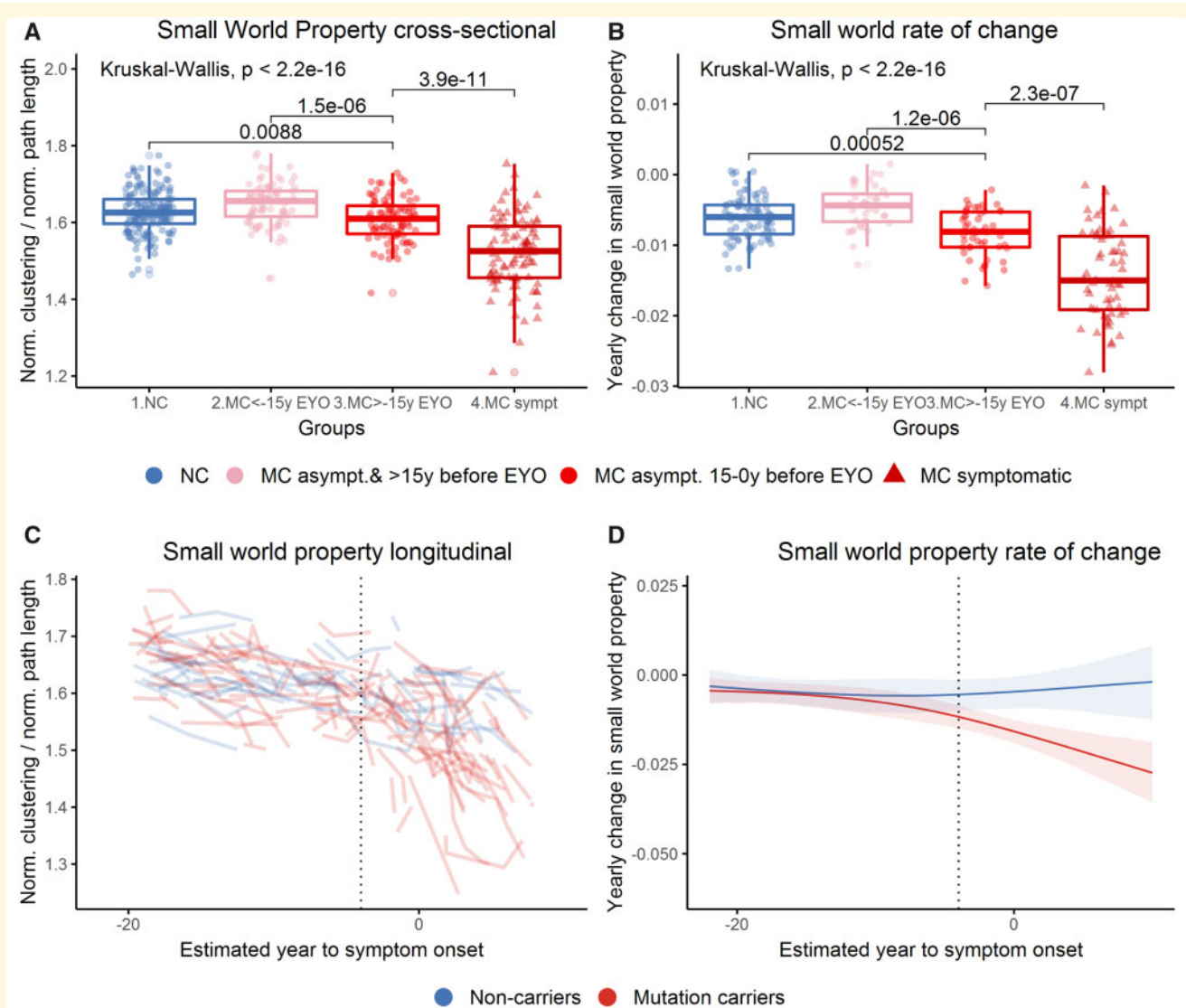


**Figure 2 Small-world coefficient for mutation carriers and non-carriers by group and rate of change by estimated year of onset.** (A, B) *P*-values based on Kruskal–Wallis, and *post hoc* Wilcoxin with Holm method correction shown for the comparison of all groups to the asymptomatic EYO between –15 and 0 mutation carriers group. No covariates included. (C, D) The fitted lines are based on all data points extending to –38 to +20. Left of EYO 0 is before expected symptom onset and right of EYO 0 is after expected symptom onset. The EYO were first jittered, and then the data points before –20 and after EYO +8 removed to avoid accidental unblinding of participants. Dotted line is the point of divergence of rate of change between mutation carriers and non-carriers.

## Discussion

Using a single-subject approach, we found that structural grey matter network properties deteriorated over the course of ADAD and that movement to a more random network topology closely correlated with cognitive decline. When comparing mutation carriers to non-affected family members global network disruptions were detected cross-sectionally as early as 12 years before expected symptom onset. Longitudinally, increased rates of decline of network metrics were evident from 6 years before expected symptom onset. In line with our hypotheses based on cross-sectional studies in sporadic Alzheimer’s disease, a lower small worldness of the network was

associated with abnormalities and decline of established markers of Alzheimer’s disease. Thus, our grey matter network analysis in this unique cohort of ADAD contributes to our understanding of the Alzheimer’s disease trajectory and indicates that our methods may potentially be a useful additional non-invasive tool for tracking disease progression.

As Alzheimer’s disease progresses, there is substantial amyloid accumulation, volumetric loss, hypometabolism and cognitive decline, but how grey matter networks fit into these processes remained unclear. Prior work in sporadic Alzheimer disease has shown that grey matter networks might be sensitive to biological changes during the preclinical stages of the disease (Tijms *et al.*, 2016;



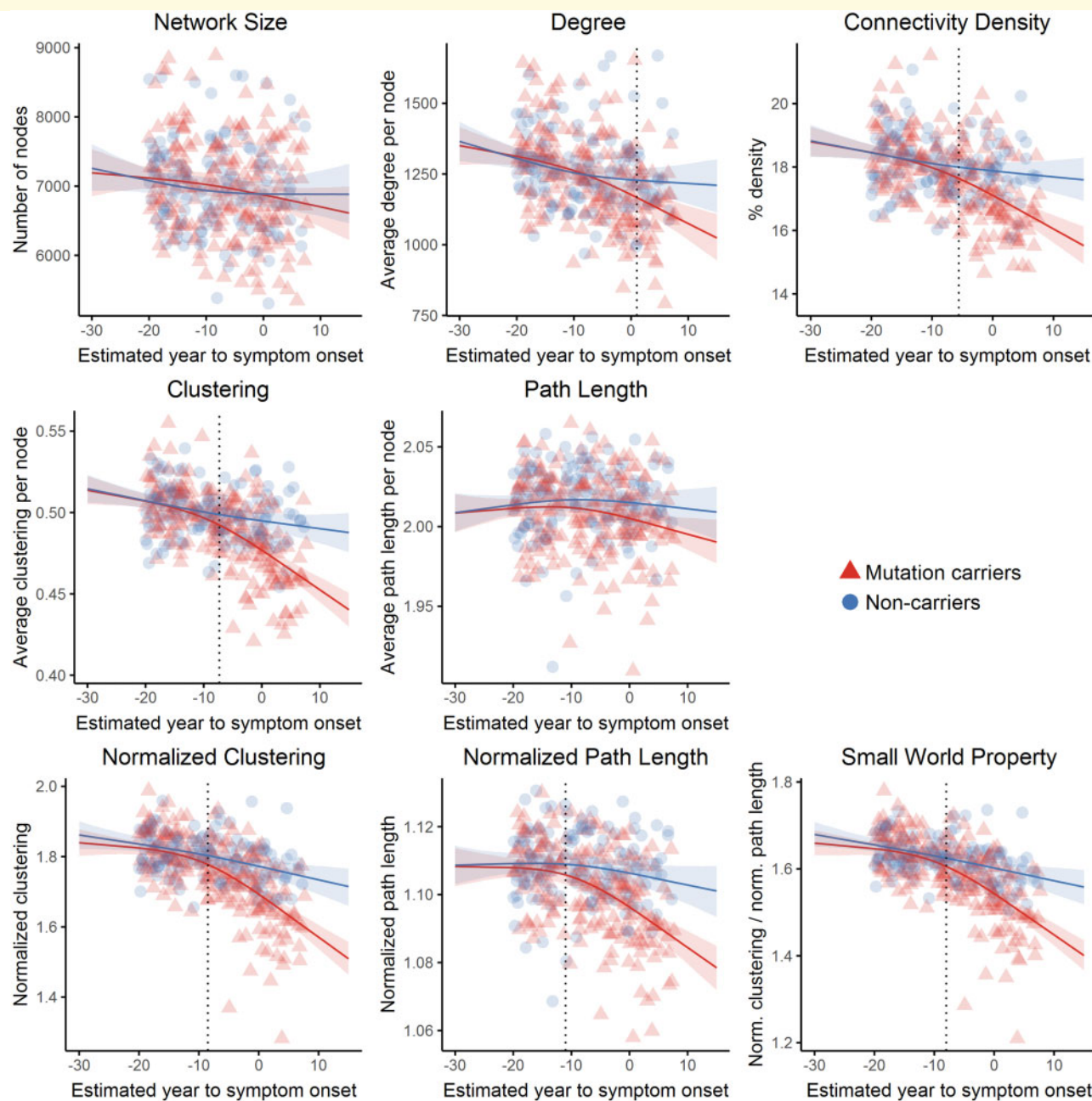


**Figure 3 Grey matter network properties by estimated year of onset at baseline between mutation carriers and non-carriers.** The fitted lines are based on all data points extending to  $-38$  to  $+20$ . Left of EYO 0 is before expected symptom onset and right of EYO 0 is after expected symptom onset. The EYO were first jittered and then the data points before  $-20$  and after EYO  $+8$  removed to avoid accidental unblinding of participants. Dotted line is the point of divergence between mutation carriers and non-carriers.  $N = 439$ .

Ten Kate *et al.*, 2018; Voevodskaya *et al.*, 2018). In the current work, we observed similar alterations of grey matter network properties in ADAD as a function of EYO. The mostly consistent changes in network properties between sporadic and ADAD strengthens the hypothesis that grey matter network disruptions are one of the downstream effects of amyloid accumulation. Using amyloid PET, we extended previous cross-sectional findings from studies in sporadic Alzheimer's disease (Ten Kate

*et al.*, 2018), by showing that higher baseline amyloid PET and higher amyloid accumulation rates are related to faster decline of grey matter network properties over time. Within asymptomatic mutation carriers only, the relationship between amyloid and the small-world coefficient was more subtle and only reached significance when studying concurrent changes of both markers, possibly due a decrease in power. The small-world summery measure was also related to sensitive markers of

Alzheimer's disease neurodegeneration and cognitive decline, in cross-sectional and longitudinal design. For these relationships, the sensitivity analyses in asymptomatic mutation carriers showed that the small-world coefficient already in early disease stages declined concurrently with other Alzheimer's disease markers. This suggested these processes occur, at least partly, in parallel (Wang et al., 2019), and support the notion that grey matter network decline is a sign of progression of Alzheimer's disease.

Previous studies in sporadic Alzheimer's disease had suggested decline over time of grey matter network integrity, as there was a decrease over disease stages cross-sectionally (Yao et al., 2010; Tijms et al., 2013b; Voevodskaya et al., 2018). Here, we show that grey matter networks properties decline over time *within* individuals, and how decline rates start to increase with disease severity. Differences between mutation carriers and non-

carriers in the *rate* of decline were generally detected later than cross-sectionally, which could have occurred because cross-sectional estimates across individuals by EYO may overestimate changes due to variance in the EYO measure (i.e. some individuals at EYO -12 are actually only 5 or 6 years from actual onset) (McDade et al., 2018). Another potential cause of cross-sectional and longitudinal estimate differences include sample sizes, with less individuals who had longitudinal data. Measurement variability over repeated measures within individuals can also have contributed to later detection of differences in the longitudinal design if these exceeded subtle rates of change. Longer follow-up time per individual in larger visit numbers is necessary for increasingly precise estimates of divergence in change over time.

Altering of network properties was not detected for every metric. This may be an indication that these metrics pick up different aspects of neurodegeneration. The small-world measures (normalized clustering, and normalized path length and small-world coefficient) showed early cross-sectional changes and seemed most sensitive to measure change over time. This is in line with network theory and previous findings in Alzheimer's disease (Tijms et al., 2018), which indicated that brain networks tend to become more similar to random networks over the disease course. The normalized network metrics reflect how different a network is from random, which may be why these best capture decline over time. Future studies are needed to confirm which network property would be the most robust summary statistic to track longitudinal grey matter network integrity in Alzheimer's disease.

On a regional level, cross-sectional network property alterations were evident earliest in the parietal regions and then spread across the brain. Most brain regions

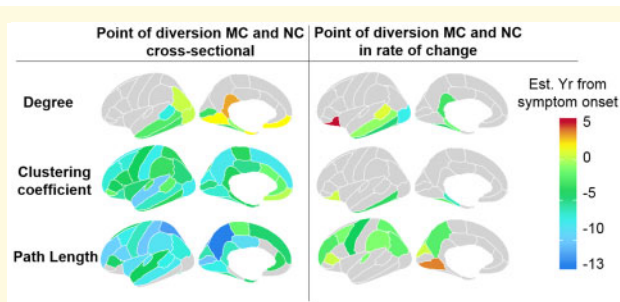


**Figure 4 Regional EYO of diversion between mutation carriers and non-carriers for grey matter network degree, clustering coefficient and path length.** Linear mixed models adjusted for sex, total grey matter volume and regional volume. MC = mutation carrier; NC = non-carrier. For details, EYO by region see [Supplementary Table 3](#).  $N = 416$ .

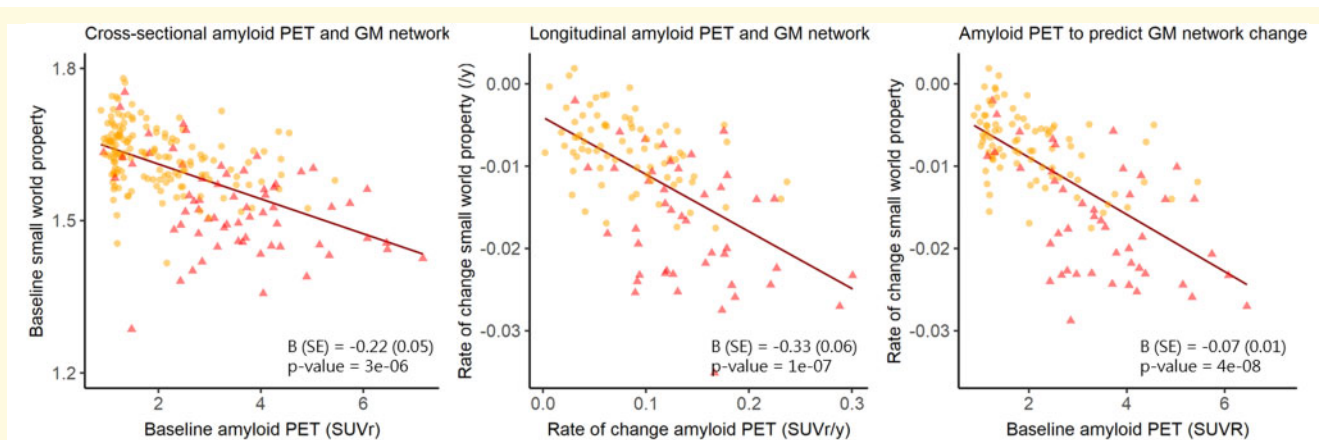
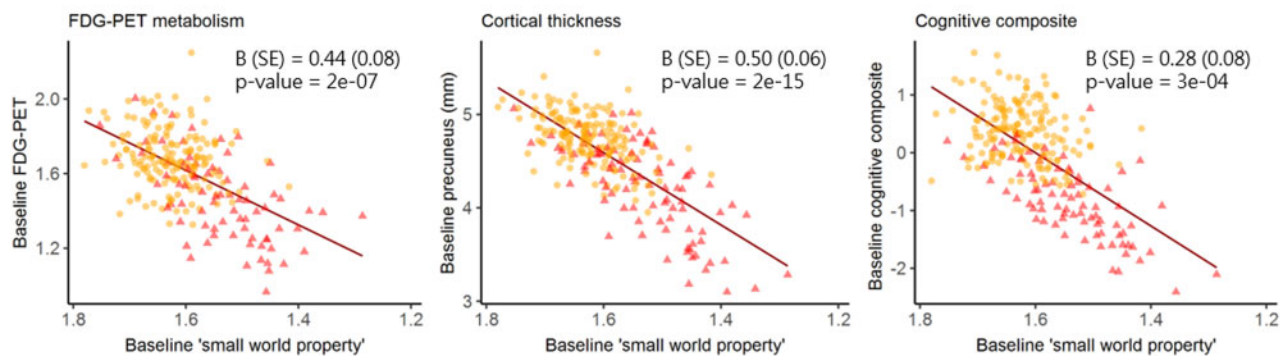
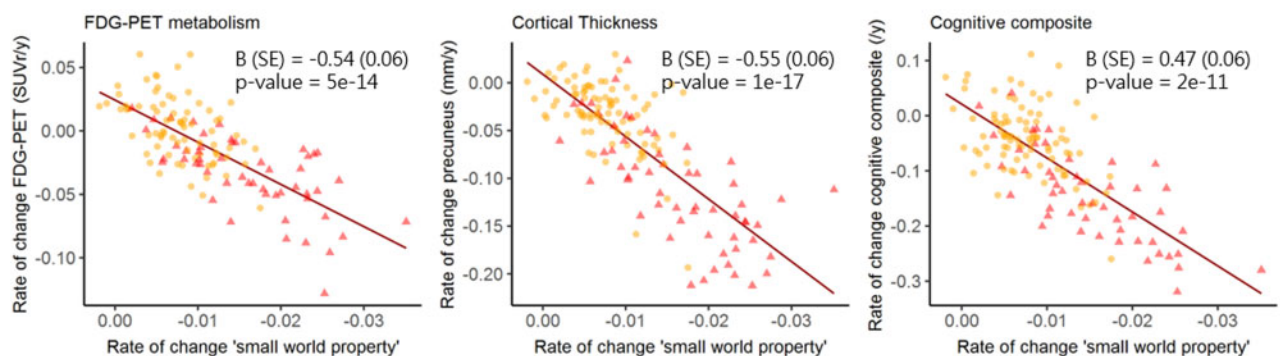


**Figure 5 Association of amyloid PET with grey matter network small-world coefficient in mutation carriers.** For visualization purposes, plotted extracted slopes with mixed model and line fitted with simple regression line in ggplot in R. Models to obtain beta and  $P$ -values specified in methods. GM network = grey matter network. Yellow circle = CDR 0 at baseline; Red triangle = CDR >0 at baseline. Amyloid PET = precuneus SUVR, Cross-sectional  $N = 222$ , Longitudinal  $N = 120$ , Predict change  $N = 131$ . For other grey matter network metrics see [Supplementary Fig. 6](#).

## Cross-sectional association with grey matter network: small world property



## Longitudinal association with grey matter network: small world property



## Predict change with baseline grey matter network: small world property

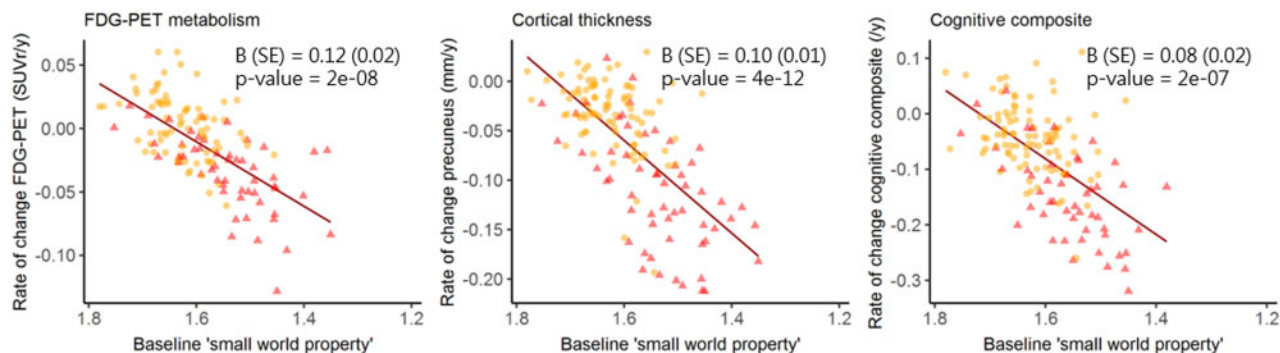


**Figure 6 Associations of grey matter network small-world coefficient with FDG-PET metabolism, cortical thickness and cognition.**

For visualization purposes, plotted extracted slopes with mixed model and line fitted with simple regression line in ggplot in R.

Models to obtain beta and  $P$ -values specified in methods. Inversed small-world coefficient to aid visualization, see also [Supplementary Table 4](#).

Yellow circle = CDR 0 at baseline; Red triangle = CDR >0 at baseline. MRI thickness = cortical thickness precuneus; FDG-PET = METAROI SUVr as described in methods. DIAN composite: equally weighted Z-score of Logical Memory Delayed Recall of the Wechsler memory test, DIAN Word List Test (comparable to International Shopping List Test), Digit Symbol Substitution Test and Mini-Mental State Examination. Cross-sectional FDG-PET  $N = 238$ , MR thickness  $N = 260$ , Cognition  $N = 251$ ; Longitudinal: FDG-PET  $N = 129$ , MR thickness  $N = 146$ , Cognition  $N = 140$ ; Predict change: FDG-PET  $N = 131$ , MR thickness  $N = 146$ , Cognition  $N = 143$ . For other grey matter network metrics see [Supplementary Figs 7–9](#).

showed a difference first for path length, then for clustering and then for degree, except for the temporal regions, in which earlier and more pronounced lowering of the clustering coefficient was seen. Regional cross-sectional patterns showed early alterations for path length and clustering in areas with most pathology in ADAD

including the precuneus. Regions of the default mode network also showed early alterations. Compared to previous sporadic Alzheimer's disease studies, we find more widely affected connectivity but the patterns are largely overlapping ([Ten Kate et al., 2018](#); [Tijms et al., 2018](#); [Verfaillie et al., 2018](#)).

Compared to other structural grey matter imaging, the cross-sectional differences in the most sensitive grey matter network metrics were detected earlier than cortical thickness and volumetric measures. It was not part of this study to investigate whether grey matter network integrity measures have the same or higher sensitivity to early alterations than other structural MRI markers. Still, we adjusted for grey matter volume to assure measuring value beyond simple volumes. The increased rates of change of network properties were detected at a similar stage to the volumetrics, and later than precuneus cortical thinning in dominantly inherited Alzheimer's disease, which is the earliest region of change (Gordon *et al.*, 2018; Kinnunen *et al.*, 2018). The results merit application of grey matter networks in future deeper investigations, for example using multimodal network approaches with white matter and functional connectivity, to better understand the substrate of cognitive decline. The observation that network disruptions increase over time in a large multicentre study is relevant for clinical trials. As the method only requires standard T<sub>1</sub> scans and the available pipeline for network calculation, a next step is to test the approach retrospectively in clinical trial populations.

One of the strengths of the current study design is the use of a previously validated method for grey matter network extraction. The unique traits of the DIAN cohort provided the ability to map changes in grey matter networks across decades of disease time. It should be noted that the estimates as a function of the expected symptom onset in dominantly inherited Alzheimer's disease are influenced by sample size. Still, this method provides a way to detect and compare changes due to Alzheimer's disease before symptom onset, and combine different families. Additionally, the rich characterization of DIAN participants provided the ability to relate observed changes in networks to other neuroimaging markers of pathology as well as cognition. A potential limitation is that our study included an average time period of 3 years in the longitudinal cohort, which may not be enough time to reliably measure changes due to Alzheimer's disease in its very early stages. Yet, we show the longitudinal analysis of structural grey matter networks alongside of the cross-sectional results, which to the best of our knowledge has not been studied before and warrants further investigation of how grey matter network integrity decreases over time in sporadic Alzheimer's disease.

In conclusion, in ADAD individual grey matter network properties are robustly associated with Alzheimer's disease severity and progression as shown by the associations with EYO, amyloid accumulation, rate of neurodegeneration and cognitive decline. These data suggest that single-subject grey matter network integrity measures obtained from structural MRI scans provide an additional, non-invasive tool for understanding and measuring progression from preclinical to severe clinical stages of Alzheimer's disease. These grey matter network

properties can reflect the asynchronous start of brain pathology following Alzheimer's disease-related cellular damage and inflammatory processes, informing about changes in grey matter covariance (Verfaillie *et al.*, 2018).

## Supplementary material

Supplementary material is available at *Brain Communications* online.

## Acknowledgements

The authors are thankful towards all research participants of the DIAN cohort and their families, as well as to all participating researchers and coordinators, and those involved in processing and sharing of the data of DIAN (<https://dian.wustl.edu/our-research/observational-study/dian-observational-study-sites/>, accessed December 2019). Data collection and sharing for this project was supported by the Dominantly Inherited Alzheimer's Network (DIAN, UF1AG032438) funded by the National Institute on Aging (NIA), the German Center for Neurodegenerative Diseases (DZNE), Raul Carrea Institute for Neurological Research (FLENI), Partial support by the Research and Development Grants for Dementia from Japan Agency for Medical Research and Development, AMED (17929884, 16815631) and the Korea Health Technology R&D Project through the Korea Health Industry Development Institute (KHIDI). This manuscript has been reviewed by DIAN Study investigators for scientific content and consistency of data interpretation with previous DIAN Study publications.

## Funding

Alzheimer Nederland Fellowship 2018 (L.V.), ZonMW Memorabel grant #73305056 (B.M.T.) and #733050824 (B.M.T. and P.J.V.). Innovative Medicine Initiative – Joint Undertaking (IMI-JU) n°115736, European Union's Seventh Framework Programme (FP7/2007–2013) (European Federation of Pharmaceutical Industries and Associations) EFPIA companies' in kind contribution (L.V., P.J.V. and P.S.). Willman Scholar Fund of the Barnes Jewish Hospital Foundation, K01 AG053474 (B.A.G.). Data collection and sharing for this project were supported by the Dominantly Inherited Alzheimer Network (DIAN) (grant no. UF1AG032438) funded by the National Institute on Aging and the German Center for Neurodegenerative Diseases (DZNE). Additional support came from the National Institutes of Health-funded National Institute of Neurological Disorders and Stroke (NINDS) Center Core for Brain Imaging (grant no. P30NS098577), the National Science Foundation (grant no. DGE-1745038), National Institutes of Health (NIH) (grant no. UL1TR001873 to J.M.N.), the Swiss National Science Foundation (grant no.

320030-160221 to J.K.), the National Institute for Health Research University College London Hospitals Biomedical Research Centre, and the Medical Research Council (MRC) Dementias Platform UK (grant nos. MR/L023784/1 and MR/009076/1). Computations were performed using the facilities of the Washington University Center for High Performance Computing, which were partially funded by National Institutes of Health (NIH) grants 1S10RR022984-01A1 and 1S10OD018091-01.

## Competing interests

C.C. receives research support from Biogen, Eisai, Alector and Parabon, and is a member of the advisory board of ADx Healthcare, Halia Therapeutics and Vivid Genomics. N. G-R. reports taking part in multicentre studies funded by Biogen, Novartis, AbbVie and Eli Lilly. J.J.H. serves as a paid consultant and/or Advisory Board member for Biogen, Takeda, Lundbeck, Eisai and Parabon. J.L. reports speaker's fees from Bayer Vital, speaker's fees from Willi Gross Foundation, consulting fees from Axon Neuroscience, consulting fees from Ionis Pharmaceuticals, non-financial support from Abbvie, outside the submitted work. E.mcd reports (research Funding); Eli Lilly- DSMB; ESAI—CMS; Alzamend—scientific advisory board. P.S. has acquired grant support (for the institution) from GE Healthcare, Danone Research, Piramal and Merck. In the past 2 years, he has received consultancy/speaker fees (paid to the institution) from Lilly, GE Healthcare, Novartis, Sanofi, Nutricia, Probiobdrug, Biogen, Roche, Avraham and EIP Pharma. Outside of this manuscript, R.J.B. reports grant/research/clinical trial support: NIH, Alzheimer's Association, BrightFocus Foundation, Rainwater Foundation Tau Consortium, Association for Frontotemporal Degeneration, Cure Alzheimer's Fund, the Tau SILK Consortium (AbbVie, Biogen, and Eli Lilly), Janssen and an anonymous foundation. R.J.B. reports consulting fees/honoraria from Janssen, Pfizer, Roche, Eisai and Merck. R.J.B. reports equity ownership interest/advisory board income from C2N Diagnostics. All other authors report no disclosures.

## References

- Aisen P, Touchon J, Amariglio R, Andrieu S, Bateman R, Breitner J, et al. EU/US/CTAD Task Force: lessons learned from recent and current Alzheimer's prevention trials. *J Prev Alzheimers Dis* 2017; 4: 116–24.
- Alexander-Bloch A, Giedd JN, Bullmore E. Imaging structural co-variability between human brain regions. *Nat Rev Neurosci* 2013a; 14: 322–36.
- Alexander-Bloch A, Raznahan A, Bullmore E, Giedd J. The convergence of maturational change and structural covariance in human cortical networks. *J Neurosci* 2013b; 33: 2889–99.
- Bassett DS, Bullmore ET. Human brain networks in health and disease. *Curr Opin Neurol* 2009; 22: 340–7.
- Bateman RJ, Benzinger TL, Berry S, Clifford DB, Duggan C, Fagan AM, the DIAN-TU Pharma Consortium for the Dominantly Inherited Alzheimer Network, et al. The DIAN-TU Next Generation Alzheimer's prevention trial: Adaptive design and disease progression model. *Alzheimers Dement* 2017; 13: 8–19.
- Bateman RJ, Xiong C, Benzinger TLS, Fagan AM, Goate A, Fox NC, et al. Clinical and biomarker changes in dominantly inherited Alzheimer's disease. *N Engl J Med* 2012; 367: 795–804.
- Bates D, Maechler M, Bolker B, Walker S. lme4: linear mixed-effects models using Eigen and S4. 2014. <http://CRAN.R-project.org/package=lme4> (March 2018, date last accessed).
- Benzinger TL, Blazey T, Jack CR, Jr., Koeppe RA, Su Y, Xiong C, et al. Regional variability of imaging biomarkers in autosomal dominant Alzheimer's disease. *Proc Natl Acad Sci U S A* 2013; 110: E4502–9.
- Carpenter B, Gelman A, Hoffman MD, Lee D, Goodrich B, Betancourt M, et al. Stan: a probabilistic programming language. *J Stat Soft* 2017; 76: 1–29.
- Chhatwal JP, Schultz AP, Johnson KA, Hedden T, Jaimes S, Benzinger TLS, for the Dominantly Inherited Alzheimer Network, et al. Preferential degradation of cognitive networks differentiates Alzheimer's disease from ageing. *Brain* 2018; 141: 1486–500.
- Desikan RS, Segonne F, Fischl B, Quinn BT, Dickerson BC, Blacker D, et al. An automated labeling system for subdividing the human cerebral cortex on MRI scans into gyral based regions of interest. *Neuroimage* 2006; 31: 968–80.
- Dicks E, Tijms BM, Ten Kate M, Gouw AA, Benedictus MR, Teunissen CE, et al. Gray matter network measures are associated with cognitive decline in mild cognitive impairment. *Neurobiol Aging* 2018; 61: 198–206.
- Donohue MC, Jacqmin-Gadda H, Le Goff M, Thomas RG, Raman R, Gamst AC, et al. Estimating long-term multivariate progression from short-term data. *Alzheimers Dement* 2014; 10 (5 Suppl): S400–10.
- Doucet GE, Moser DA, Rodrigue A, Bassett DS, Glahn DC, Frangou S. Person-based brain morphometric similarity is heritable and correlates with biological features. *Cereb Cortex* 2019; 29: 852–62.
- Draganski B, Gaser C, Busch V, Schuierer G, Bogdahn U, May A. Neuroplasticity: changes in grey matter induced by training. *Nature* 2004; 427: 311–2.
- Fischl B. FreeSurfer. *Neuroimage* 2012; 62: 774–81.
- Franzmeier N, Duzel E, Jessen F, Buerger K, Levin J, Duering M, et al. Left frontal hub connectivity delays cognitive impairment in autosomal-dominant and sporadic Alzheimer's disease. *Brain* 2018; 141: 1186–200.
- Gelman A, Lee D, Guo JQ. Stan: a probabilistic programming language for Bayesian inference and optimization. *J Educ Behav Stat* 2015; 40: 530–43.
- Gordon BA, Blazey TM, Su Y, Hari-Raj A, Dincer A, Flores S, et al. Spatial patterns of neuroimaging biomarker change in individuals from families with autosomal dominant Alzheimer's disease: a longitudinal study. *Lancet Neurol* 2018; 17: 241–50.
- He Y, Chen Z, Evans A. Structural insights into aberrant topological patterns of large-scale cortical networks in Alzheimer's disease. *J Neurosci* 2008; 28: 4756–66.
- He Y, Chen ZJ, Evans AC. Small-world anatomical networks in the human brain revealed by cortical thickness from MRI. *Cereb Cortex* 2007; 17: 2407–19.
- Humphries MD, Gurney K. Network 'small-world-ness': a quantitative method for determining canonical network equivalence. *PLoS One* 2008; 3: e0002051.
- Jack CR, Jr., Bennett DA, Blennow K, Carrillo MC, Dunn B, Haeberlein SB, et al. NIA-AA research framework: toward a biological definition of Alzheimer's disease. *Alzheimers Dement* 2018; 14: 535–62.
- Jack CR, Jr., Bernstein MA, Borowski BJ, Gunter JL, Fox NC, Thompson PM, et al. Update on the magnetic resonance imaging core of the Alzheimer's disease neuroimaging initiative. *Alzheimers Dement* 2010; 6: 212–20.

- Kim HJ, Shin JH, Han CE, Kim HJ, Na DL, Seo SW, et al. Using individualized brain network for analyzing structural covariance of the cerebral cortex in Alzheimer's patients. *Front Neurosci* 2016; 10: 394.
- Kinnunen KM, Cash DM, Poole T, Frost C, Benzinger TLS, Ahsan RL, Dominantly Inherited Alzheimer Network (DIAN), et al. Presymptomatic atrophy in autosomal dominant Alzheimer's disease: a serial magnetic resonance imaging study. *Alzheimers Dement* 2018; 14: 43–53.
- Landau SM, Harvey D, Madison CM, Koeppe RA, Reiman EM, Foster NL, et al. Associations between cognitive, functional, and FDG-PET measures of decline in AD and MCI. *Neurobiol Aging* 2011; 32: 1207–18.
- Li Y, Wang Y, Wu G, Shi F, Zhou L, Lin W, et al. Discriminant analysis of longitudinal cortical thickness changes in Alzheimer's disease using dynamic and network features. *Neurobiol Aging* 2012; 33: 427.e15.
- Maslov S, Sneppen K. Specificity and stability in topology of protein networks. *Science* 2002; 296: 910–3.
- McDade E, Wang G, Gordon BA, Hassenstab J, Benzinger TLS, Buckles V, for the Dominantly Inherited Alzheimer Network, et al. Longitudinal cognitive and biomarker changes in dominantly inherited Alzheimer disease. *Neurology* 2018; 91: e1295–306.
- Mechelli A, Friston KJ, Frackowiak RS, Price CJ. Structural covariance in the human cortex. *J Neurosci* 2005; 25: 8303–10.
- Mishra S, Blazey TM, Holtzman DM, Cruchaga C, Su Y, Morris JC, et al. Longitudinal brain imaging in preclinical Alzheimer disease: impact of APOE epsilon4 genotype. *Brain* 2018; 141: 1828–39.
- Morris JC. The Clinical Dementia Rating (CDR): current version and scoring rules. *Neurology* 1993; 43: 2412–4.
- Oxtoby NP, Young AL, Cash DM, Benzinger TLS, Fagan AM, Morris JC, et al. Data-driven models of dominantly-inherited Alzheimer's disease progression. *Brain* 2018; 141: 1529–44.
- Roe CM, Ances BM, Head D, Babulal GM, Stout SH, Grant EA, et al. Incident cognitive impairment: longitudinal changes in molecular, structural and cognitive biomarkers. *Brain* 2018; 141: 3233–48.
- Rubinov M, Sporns O. Complex network measures of brain connectivity: uses and interpretations. *Neuroimage* 2010; 52: 1059–69.
- Ryman DC, Acosta-Baena N, Aisen PS, Bird T, Danek A, Fox NC, the Dominantly Inherited Alzheimer Network, et al. Symptom onset in autosomal dominant Alzheimer disease: a systematic review and meta-analysis. *Neurology* 2014; 83: 253–60.
- Scheltens P, Blennow K, Breteler MM, de Strooper B, Frisoni GB, Salloway S, et al. Alzheimer's disease. *Lancet* 2016; 388: 505–17.
- Seeley WW, Crawford RK, Zhou J, Miller BL, Greicius MD. Neurodegenerative diseases target large-scale human brain networks. *Neuron* 2009; 62: 42–52.
- Seidlitz J, Vasa F, Shinn M, Romero-Garcia R, Whitaker KJ, Vertes PE, et al. Morphometric similarity networks detect microscale cortical organization and predict inter-individual cognitive variation. *Neuron* 2018; 97: 231–47.e7.
- Su Y, Blazey TM, Snyder AZ, Raichle ME, Marcus DS, Ances BM, et al. Partial volume correction in quantitative amyloid imaging. *Neuroimage* 2015; 107: 55–64.
- Su Y, D'Angelo GM, Vlassenko AG, Zhou GF, Snyder AZ, Marcus DS, et al. Quantitative analysis of PiB-PET with FreeSurfer ROIs. *PLOS One* 2013; 8: e73377.
- Ten Kate M, Visser PJ, Bakardjian H, Barkhof F, Sikkes SAM, van der Flier WM, et al. Gray matter network disruptions and regional amyloid beta in cognitively normal adults. *Front Aging Neurosci* 2018; 10: 67.
- Tijms BM, Kate MT, Wink AM, Visser PJ, Ecay M, Clerigie M, et al. Gray matter network disruptions and amyloid beta in cognitively normal adults. *Neurobiol Aging* 2016; 37: 154–60.
- Tijms BM, Moller C, Vrenken H, Wink AM, de Haan W, van der Flier WM, et al. Single-subject gray matter graphs in Alzheimer's disease. *PLoS One* 2013a; 8: e58921.
- Tijms BM, Series P, Willshaw DJ, Lawrie SM. Similarity-based extraction of individual networks from gray matter MRI scans. *Cereb Cortex* 2012; 22: 1530–41.
- Tijms BM, Ten Kate M, Gouw AA, Borta A, Verfaillie S, Teunissen CE, et al. Gray matter networks and clinical progression in subjects with predementia Alzheimer's disease. *Neurobiol Aging* 2018; 61: 75–81.
- Tijms BM, Wink AM, de Haan W, van der Flier WM, Stam CJ, Scheltens P, et al. Alzheimer's disease: connecting findings from graph theoretical studies of brain networks. *Neurobiol Aging* 2013b; 34: 2023–36.
- Verfaillie SCJ, Slot RER, Dicks E, Prins ND, Overbeek JM, Teunissen CE, et al. A more randomly organized grey matter network is associated with deteriorating language and global cognition in individuals with subjective cognitive decline. *Hum Brain Mapp* 2018; 39: 3143–51.
- Vermunt L, Sikkes SAM, van den Hout A, Handels R, Bos I, van der Flier WM, et al. Duration of preclinical, prodromal, and dementia stages of Alzheimer's disease in relation to age, sex, and APOE genotype. *Alzheimers Dement* 2019; 15: 888–98.
- Villemagne VL, Burnham S, Bourgeat P, Brown B, Ellis KA, Salvado O. Amyloid beta deposition, neurodegeneration, and cognitive decline in sporadic Alzheimer's disease: a prospective cohort study. *Lancet Neurol* 2013; 12: 357–67.
- Voevodskaya O, Pereira JB, Volpe G, Lindberg O, Stomrud E, van Westen D, et al. Altered structural network organization in cognitively normal individuals with amyloid pathology. *Neurobiol Aging* 2018; 64: 15–24.
- Wang G, Coble D, McDade EM, Hassenstab J, Fagan AM, Benzinger TLS, and the Dominantly Inherited Alzheimer Network (DIAN), et al. Staging biomarkers in preclinical autosomal dominant Alzheimer's disease by estimated years to symptom onset. *Alzheimers Dement* 2019; 15: 506–14.
- Yao Z, Zhang Y, Lin L, Zhou Y, Xu C, Jiang T, the Alzheimer's Disease Neuroimaging Initiative. Abnormal cortical networks in mild cognitive impairment and Alzheimer's disease. *PLoS Comput Biol* 2010; 6: e1001006.
- Young AL, Oxtoby NP, Daga P, Cash DM, Fox NC, Ourselin S, et al. A data-driven model of biomarker changes in sporadic Alzheimer's disease. *Brain* 2014; 137: 2564–77.
- Zielinski BA, Gennatas ED, Zhou J, Seeley WW. Network-level structural covariance in the developing brain. *Proc Natl Acad Sci U S A* 2010; 107: 18191–6.

## Appendix I. The dominantly inherited Alzheimer's network

Ricardo Allegri, Fatima Amtashar, Tammie Benzinger, Sarah Berman, Courtney Bodge, Susan Brandon, William Brooks, Jill Buck, Virginia Buckles, Sochenda Chea, Patricio Chrem, Helena Chui, Jake Cinco, Clifford Jack, Mirelle D'Mello, Tamara Donahue, Jane Douglas, Noelia Edigo, Nilufer Erekin-Taner, Anne Fagan, Marty Farlow, Angela Farrar, Howard Feldman, Gigi Flynn, Nick Fox, Erin Franklin, Hisako Fujii, Cortaiga Gant, Samantha Gardener, Bernardino Ghetti, Alison Goate, Jill Goldman, Brian Gordon, Julia Gray, Jenny Gurney, Jason Hassenstab, Mie Hirohara, David Holtzman, Russ Hornbeck,

Siri Houeland DiBari, Takeshi Ikeuchi, Snezana Ikonovic, Gina Jerome, Mathias Jucker, Kensaku Kasuga, Takeshi Kawarabayashi, William Klunk, Robert Koeppe, Elke Kuder-Buletta, Christoph Laske, Johannes Levin, Daniel Marcus, Ralph Martins, Neal Scott Mason, Denise Maue-Dreyfus, Eric McDade, Lucy Montoya, Hiroshi Mori, Akem Nagamatsu, Katie Neimeyer, James Noble, Joanne Norton, Richard Perrin, Marc Raichle, John Ringman, Jee Hoon Roh, Peter Schofield, Hiroyuki Shimada, Tomoyo Shiroto, Mikio Shoji, Wendy Sigurdson, Hamid Sohrabi, Paige Sparks, Kazushi Suzuki, Laura Swisher, Kevin Taddei, Jen Wang, Peter Wang, Mike Weiner, Mary Wolfsberger, Chengjie Xiong and Xiong Xu.